Nanoscale Advances

View Article Online
DOI: 10.1039/D5NA00919G

Exfoliation and transfer of millimetre-sized MoS_2 flakes on arbitrary substrates

Riccardo Galafassi,[*,†,‡,‖] Ermes Peci,[¶,‖] Valentina Venturino,[¶] Michele Magnozzi,[¶] Francesca Telesio,[§] Maurizio Canepa,[¶] and Francesco Bisio[†]

†*CNR-SPIN, Corso Perrone 24, 16152 Genova, Italy*

‡*RAISE Ecosystem, Genova, Italy*

¶*Optmatlab, Dipartimento di Fisica, Università degli Studi di Genova, Via Dodecaneso 33, 16146 Genova*

§*Dipartimento di Fisica, Università degli Studi di Genova, Via Dodecaneso 33, 16146 Genova*

‖*These authors contributed equally to this work*

E-mail: riccardo.galafassi@cnr.it

Abstract

Two-dimensional (2D) materials have the potential to strongly and sustainably influence technological development in the fields of optoelectronics, energy production and management, catalysis and more. One limiting factor that presently prevents the full exploitation of these materials is, however, the difficulty of obtaining large-scale, high-quality 2D samples on arbitrary substrates. In this work, we introduce a significant generalization of previously reported gold-assisted exfoliation techniques of TMDCs, marking a step forward towards the fabrication of macroscopic 2D materials samples on arbitrary substrates. We achieved the successful production of millimetre-sized monolayer MoS_2 onto silica, PDMS, and both thermal and native oxidized silicon

View Article Online
DOI: 10.1039/D5NA00919G

wafers. Moreover, our method simplifies previously reported gold-assisted exfoliation methods by removing substrate functionalization procedures and complex steps to achieve a reliable and reproducible procedure. The crystal quality of the monolayers was probed using XPS, Raman and photoluminescence revealing a negligible presence of contaminants and defects in the samples. Furthermore, using imaging ellipsometry, we could investigate, on the millimetre scale, the samples morphology and the selectivity of the exfoliation process to produce single layer MoS_2 flakes. Finally, we further extended the capability of our exfoliation method by enabling the seamless transfer of large-area samples from PDMS to advanced substrates, unlocking new possibilities for large-scale 2D devices fabrication.

Introduction

Ever since the first isolation of graphene[1], 2-dimensional (2D) materials have become almost ubiquitous in condensed matter physics due to their amazing physical properties and ease of fabrication[2]. Among the large family of 2D materials, group-VI transition metal dichalcogenides (TMDCs) have drawn a particular interest due to their semiconducting nature, excellent optoelectronic properties and widespread availability[3]. Their 2D character promotes indeed the appearance of unique properties, among which the indirect-to-direct band gap transition when going from bulk to monolayer[4], very high exciton binding energies[5] and spin-valley coupling in the electronic structure[6]. A wide range of possible applications arise from these outstanding properties, laying the ground for a possible technological revolution in fields such as electronics, optics, and computing[7,8].

One of the major obstacles for the full exploitation of 2D systems has always been the lack of a scalable and reliable method for the deterministic production of spatially extended and high-quality monolayers. The most widely employed fabrication methods, such as the mechanical *scotch tape method*[1], the liquid phase exfoliation[9], and the chemical vapor deposition[10], all exhibit some intrinsic drawbacks in terms of either yield, scalability, or sample

View Article Online
DOI: 10.1039/D5NA00919G

quality. Recent studies have shown great progress in this direction, reporting for example the wafer-scale growth of 2D materials, albeit with multiple translational grain boundaries[11–13]; a recently reported method based on 2D Czochralski growth also promises to address these issues by producing almost defect-free extended monolayers[14], but the true scalability and universality of these methods is yet to fully prove.

In general terms, however, the conceptual and practical simplicity of the mechanical exfoliation method remains unparalleled; for this reason, great curiosity surrounded the report of the breakthrough achievement of extended TMDC monolayer fabrication obtained by introducing metallic layers to complement the conventional *scotch-tape* method[15–22]. The rationale behind this innovative approach is to perform the mechanical exfoliation of the TMDC from the parent crystal not directly by tape, but by means of a metallic layer, whose adhesion to the TMDC surface is stronger than the TMDC's interlayer adhesion[15]. Experiments showed that large ML TMDC areas could be peeled from the parent crystal in this way, significantly improving with respect to the original metal-free version.

Following early implementations[16,17,23], the metal-assisted exfoliation has been gradually improved and refined[19,20,24], to the point of producing high-quality millimetre-sized monolayer TMDCs on selected substrates. The interaction between gold surfaces and TMDCs has been described in various ways[24]. Some studies characterize it as 'covalent-like quasi-bonding'[25,26] or 'mixed vdW–covalent'[27], while others refer to it as physisorption/chemisorption[28] or simply as a 'strong' interaction[15,29–32]. The roles of strain[33,34] and electrostatics[35] have been investigated. Beyond gold, several other metals have been shown to effectively exfoliate a variety of 2D materials[36–38]. Nevertheless, gold remains the primary focus of most studies, as it is resistant to oxidation and can be readily grown[27].

Liu *et al.*, in particular, perfected the gold-mediated exfoliation to the point of exfoliating large-area ML samples onto non-metallic substrates[39], seemingly addressing the issues and limitations that were present in early works. A crucial aspect of their procedure was the exploitation of a thermal release tape (TRT) as a vector to mechanically sustain the sacrificial

View Article Online
DOI: 10.1039/D5NA00919G

Au layer during the exfoliation of the TMDC and the transfer toward the target substrate. Upon pressing the TRT/Au/TMDC on a substrate of choice, the TRT was released by heating the system, and the sacrificial-layer was etched, leaving the TMDC ML behind. A later work by Petrini *et al.*[40], however, despite strictly adhering to Liu's recipe, reported a systematic cracking and wrinkling of the metal layer due to heat-induced stress of the TRT polymer, resorting to functionalize the target substrate with (3-Aminopropyl)triethoxysilane (APTES) in order to increase the adhesive force between the substrate and the TMDCs and circumvent the issue[40]. The procedure, albeit introducing an extra fabrication step, ensured an improved mechanical stability of the TMDC/metal stack and successfully yielded large-area monolayers of TMDC, incidentally promoting a stronger adhesion to the target substrate, a factor that may be beneficial in subsequent processes that require sample sonication[41] or detrimental when further transfer is required.

In order to be able to fabricate large-area ML flakes of TMDCs on a large variety of substrates, and leave open the possibility to further transfer them onto other systems, we developed an improved version of the sacrificial gold layer-assisted exfoliation methods so far reported[39,40] that significantly extends the range of applicability of large-scale exfoliation of TMDCs. In detail, the surface functionalization of the target substrate was replaced with a simple reversible mechanical constraint, a rigid PDMS layer, introduced during the critical TRT-release stage, thereby altogether avoiding the need of intermediate additional chemical processes and of additional fabrication steps that might compromise the sample quality. With this approach, we demonstrated the possibility to achieve large-area TMDC MLs on substrates as diverse as Si wafers with native (2 nm) and thermal (300 nm) oxide, bulk fused silica and polydimethylsiloxane (PDMS). Moreover, exploiting the successful exfoliation on PDMS, which distinguish our method from nearly the totality of the reported metal-assisted exfoliation methods, we demonstrated that large-area ML TMDC flakes could be further deterministically transferred on a wide variety of other substrates with microscopic control on the crystal positioning, exploiting well-established PDMS-based dry-transfer methods[42,43].

View Article Online
DOI: 10.1039/D5NA00919G

Exfoliation of large-area monolayer MoS_2

In this work, we focused on a natural crystal of MoS_2 as parent bulk material for the exfoliation, since the generalization to the many other 2D materials that are compatible with gold-assisted exfoliation is straightforward[25,39]. Since substrate compatibility was reported to be a delicate issue within existing gold-assisted exfoliation reports[40], we chose to address different target substrates, namely: **i.** P-type silicon (resistivity $\sim$20 Ω cm) with native SiO_2 oxide (SiO_2(nat)/Si); **ii.** N-type silicon (resistivity $\sim$20 Ω cm) with a thermally grown SiO_2 layer (SiO_2(285 nm)/Si); **iii.** fused silica; **iv.** Polydimethylsiloxane (Sylgard 184 with a 10:1 cross-linker/curing agent ratio), chosen as representative of different domains of future applications in the fields of electronics, optics and flexible devices. The choice of the doping type for the silicon wafers was mainly driven by the availability of the silicon wafers.

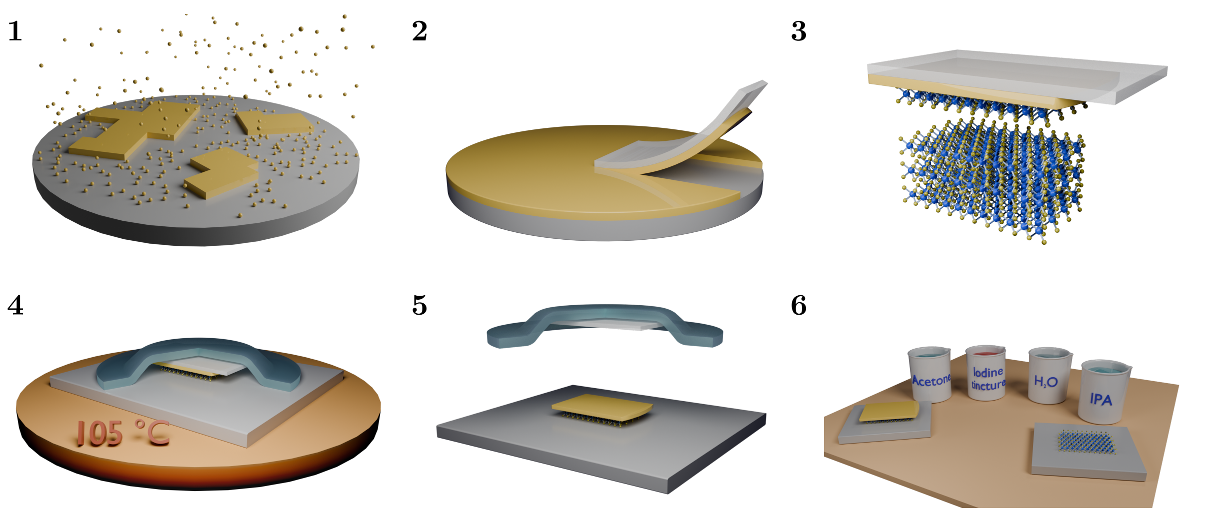

Figure 1: Step-by-step schematic representation of the exfoliation process. **(1)** A 150 nm thick gold film is deposited via sputtering on a silicon wafer. **(2)** Part of the gold layer is peeled off from the wafer by means of the TRT. **(3)** The gold/TRT stack is exploited to exfoliate a MoS_2 monolayer from the bulk crystal. **(4)** The MoS_2/Au/TRT system is laid on the desired substrate, pressed with a PDMS layer (light blue) and heated to promote the detachment of the TRT. **(5)** the MoS_2/Au stack is detached from the TRT. **(6)** The gold layer is etched by sequentially dipping the substrate/MoS_2/Au system in acetone, iodine tincture, H_2O and IPA.

Figure 1 shows the different steps of the exfoliation process. **(1)** A 150 nm-thick gold film

View Article Online
DOI: 10.1039/D5NA00919G

was deposited via sputtering on a Si wafer previously cleaned in oxygen plasma for 5 minutes at 50 W in order to remove contaminants on the surface; no adhesion layer was deposited in order to ensure an easy peeling in the subsequent step. **(2)** A Nitto Denko Revalpha RA-95LS(N) thermal release tape (TRT) was then placed directly on the gold coated wafer and used to pick up a centimetre-sized piece of the gold film from the silicon wafer. **(3)** The TRT-supported gold film was pressed onto a freshly cleaved bulk MoS_2 crystal. This step was performed in the shortest time possible, in order to prevent the contamination of the gold surface and the MoS_2 crystal from ambient air[44]. The TRT/Au stack was then peeled off the bulk MoS_2, stripping a monolayer MoS_2 in the process, and pressed onto the target substrate of choice.

At this stage, in order to release the sample, the TRT needs to be heated above 105 °C; normally, this results in the TRT bending away from the underlying substrate, lifting the thin MoS_2/Au layer and preventing their transfer[40].

In this work, we prevented the detrimental TRT buckling by **(4)** fully covering the MoS_2/Au/TRT system by means of an adhesive rigid layer, thereby providing a mechanical constraint for the TRT and allowing it to lose adhesion while simultaneously maintaining the Au/MoS_2 assembly firmly in contact with the substrate. For our experiments, the constraint layer consisted of 1.5-mm-thick PDMS, that ensured surface cleanliness and prevented sample contamination. The PDMS was prepared using Sylgard 184 with a 10:1 cross-linker/curing agent ratio cured for 24 hours at 60°C. The PDMS was placed directly on the MoS_2/Au/TRT stack upon cutting a large enough region to fully cover the sample. **(5)** The PDMS/TRT stack was then removed, leaving the Au/MoS_2/substrate system behind, and **(6)** the gold layer was dissolved by standard Au-etching procedures: the sample was first washed in acetone for a few minutes to remove any organic contamination from the tape, then the gold layer was etched using iodine tincture (1:4:40 I_2:KI:H_2O) and washed in DI water, in IPA, and finally dried using dry nitrogen.

Steps **(2)** to **(4)** were performed under controlled nitrogen atmosphere in order to mini-

View Article Online
DOI: 10.1039/D5NA00919G

mize the humidity level during the exfoliation procedure, effectively reducing airborne contamination of the Au/MoS_2 interface and consequently improving the exfoliation throughput[44–46].

In SI, Figure S1 shows photos of the various steps of exfoliation procedure.

Imaging ellipsometry of large-scale monolayers

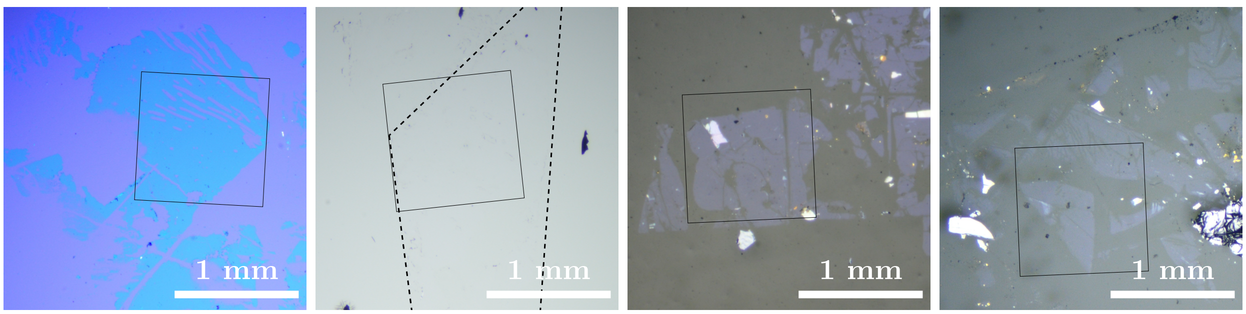

(a) SiO_2(285 nm)/Si (b) SiO_2(nat)/Si (c) PDMS (d) Silica

Figure 2: Optical microscopy of the samples exfoliated on different substrates, as indicated in the panel caption. The black rectangles indicate the area where imaging ellipsometry measurements were performed. In panel (b), where optical contrast is negligible, a black dashed line marks the approximate outline of the sample.

In Figure 2 we show optical microscopy images of one representative sample for each substrate type. The samples on SiO_2(285 nm)/Si, fused silica and PDMS exhibit an optical contrast sufficiently high to be located under a normal optical microscope, while the flakes exfoliated on Si wafers with native oxide are not readily observable, as indeed expected.

In order to overcome this complication and, above all, to quantitatively assess the sample morphology, we performed imaging spectroscopic ellipsometry (iSE) measurements, which allow to probe the optical properties of 2D materials[48–50] and to readily detect sample thickness variations with sub-nanometre precision, unambiguously identifying the number of exfoliated layers[51] of TMDC systems. Moreover, in contrast with atomic force microscopy (AFM) which has proved to be inefficient in measuring the thickness of monolayer samples[52,53], iSE thickness measurements are unaffected by the eventual presence of contaminants and by

View Article Online
DOI: 10.1039/D5NA00919G

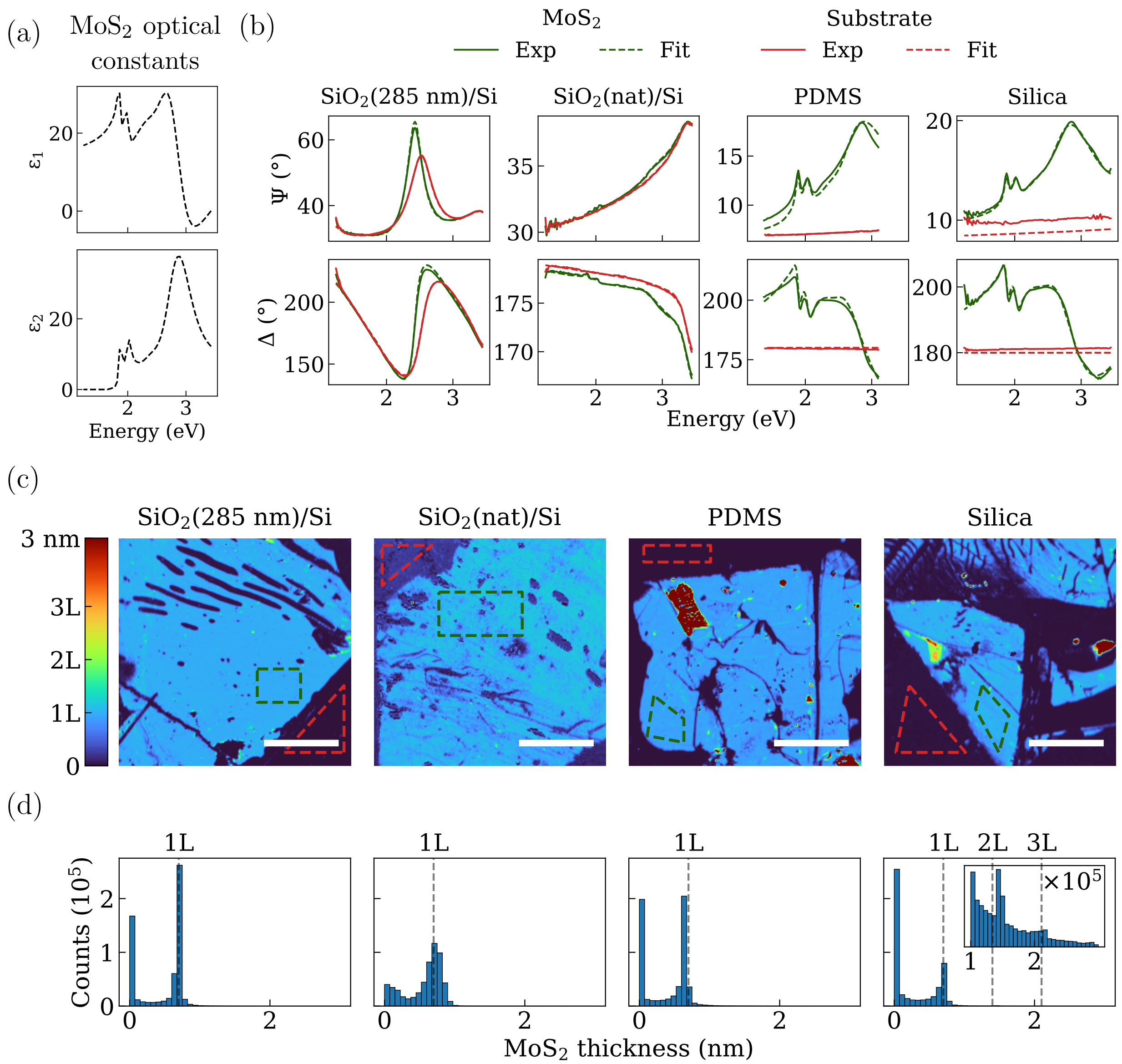

Figure 3: (a) Optical constants of the MoS_2 used in the modelling[47]. (b) Experimental data (solid lines) and best fits (dashed lines) of the ellipsometric angles $\Psi(\lambda)$ and $\Delta(\lambda)$ averaged over the dashed-line regions of (c). The green lines correspond to MoS_2-covered regions, whereas the dark-red ones indicate the respective substrates. (c) MoS_2 thickness maps extracted from the analysis of the imaging ellipsometric measurements. Light blue areas correspond to exfoliated MoS_2 areas. Dark red regions in the samples on PDMS and silica indicate the presence of thick multilayer regions. The scale bar is 300 µm for all the images. (d) MoS_2-thickness histograms corresponding to the maps in (c). The peaks at 0 nm and ~ 0.7 nm correspond to the substrate and the monolayer MoS_2 (1L), respectively. Some small bilayer ~ 1.4 nm (2L) and trilayer ~ 2.1 nm (3L) regions are also observed in the sample on silica as shown in the inset.

View Article Online
DOI: 10.1039/D5NA00919G

the interaction with the substrate that may lead to anomalous thickness values using AFM. Instead, the latter was used to image the surface topography and acquire information on the surface morphology of the samples. Figure S4 displays the AFM mapping of a sample on SiO_2(nat)/Si, showing the absence of contaminants on the MoS_2 surface, beside small unavoidable dust particles. Hyperspectral iSE measurements were performed mapping the ellipsometric angles $\Psi(\lambda)$ and $\Delta(\lambda)$ at 129 different wavelengths spanning the near-UV, visible and near-infrared range, as detailed in the Methods section. A few representative such maps are reported in Figure S2 and Figure S3.

The experimental data were subsequently analysed by means of a layer-stack model that included, bottom to top, a semi-infinite substrate, a SiO_2 layer (where applicable) and a MoS_2 layer with parametrized complex dielectric function adapted from our previous work[47] (Figure 3a). For the latter, the tabulated optical constants can be found in SI in Table S1. The full description of the model used for each system can be found in Figure S5. Continuous lines in Figure 3b show the values of Ψ and Δ as a function of the energy of the incoming light, averaged over the homogeneous regions highlighted by the dashed polygons in Figure 3c. The bare-substrate spectra are reported as the dark-red lines, whereas the MoS_2-covered areas are reported as the green spectra. The differences between the spectra collected on different substrates are readily understandable based on the respective differences in dielectric function and morphology. In all the MoS_2-covered spectra, variations of different magnitude with respect to the spectra on the bare substrate are observed, whose extent and spectral shape depended upon the dielectric mismatch of MoS_2 and substrate material. The optical model parameters were optimized to best fit the experimental data, finding a good agreement between models and data. The resulting fit curves are represented by dashed lines in Figure 3b for each system.

Using these models, we performed a pixel-by-pixel fitting of the iSE maps, leaving the MoS_2 thickness as the only free-fit parameter. The resulting thickness maps are shown in Figure 3c, and the corresponding thickness histograms are displayed in Figure 3d. The

View Article Online
DOI: 10.1039/D5NA00919G

thickness maps clearly show that, beside some inhomogeneous areas, all the substrates under consideration feature large-area uniform monolayer MoS_2 regions, with lateral dimensions ranging from hundreds of microns to mm. Small bilayer, trilayer and bulk regions are present on the silica and PDMS substrates, but overall it is apparent that the method is able to produce large area monolayer MoS_2 samples on different substrates. iSE, beside confirming the monolayer nature of the exfoliated samples on $\sim$mm$\times$mm regions allowed to enhance the visibility compared to the optical images in Figure 2 enhancing the contrast between the MoS_2 and the substrate on all the substrates. This is of particular interest for SiO_2(nat)/Si, PDMS and silica where the flakes are invisible or barely visible.

Structural, chemical and photonic properties

Once we have ascertained the presence of large-area MoS_2 flakes, we proceeded to assess their structural, chemical and photonic characteristics, by means of X-ray photoemission spectroscopy (XPS), Raman spectroscopy and photoluminescence (PL).

Figure 4a shows the XPS survey spectra of large-area MoS_2 over the four different substrates. The S/Mo ratio was extracted from the spectra in Figure 4a obtaining a ratio of 1.9 ± 0.1 and 2.0 ± 0.1 for the samples on SiO_2(nat)/Si and SiO_2(285 nm)/Si respectively (please see the SI for more details). All the spectra exhibit prominent Si, S, Mo, C, and O peaks due to the MoS_2 (Mo and S), the substrates (Si and O, and C in the case of PDMS) and adventitious contamination (C). Traces of iodine due to the etching solution can be found on the SiO_2(285 nm)/Si sample and on the PDMS sample. In particular, PDMS substrates undergoing the etching procedure turn slightly yellow after being in contact with the etchant, suggesting a reaction with PDMS that, however, does not alter its viscoelastic properties. The Si 2p peaks of the SiO_2(nat.)/Si sample are split into low-BE components (pure Si) and a high-BE components (SiO_2).

Figure 4b shows high resolution (HR) XPS spectra of the four samples, performed in the

View Article Online
DOI: 10.1039/D5NA00919G

energy ranges corresponding to the Mo 3p/N 1s, Mo 3d/S 2s, S 2p, and C 1s peaks. The HR spectra were deconvolved into their chemically-shifted subcomponents as detailed in the Methods section. In general, the XPS spectra in corresponding energy regions share similar structures. The binding energies (BE) of the Mo 3p, Mo 3d, N 1s, S 2s and S 2p peaks are all reported in Table 1. The binding energy was referenced to Mo $3d_{5/2}$ at 229.5 eV, since C 1s referencing is not appropriate for comparing data across these substrates[54]. From the deconvolution procedure, we can observe that the Mo $3d_{5/2}/3d_{3/2}$ peak is composed of a single doublet, unambiguously indicating that only the Mo(IV) states involved in MoS_2 are present, and justifying the energy referencing. The broad feature centred around 416 eV BE (hatched area) can be attributed to plasmon losses. Similarly, the absence of further components near the S $2p_{3/2}/2p_{1/2}$ doublet confirms that sulphur is not involved in chemical bonds other than MoS_2. The larger FWHM of the peaks (especially the S 2p) for the PDMS sample is ascribed to the superposition of contributions from monolayer and few-layer areas, given that the XPS measuring spot has few-hundred micron of lateral dimension. The N 1s peak around 399 eV BE testifies the presence of very small quantities of nitrogen, that can, however, be observed in the bare substrates. Figure S6 shows the XPS survey spectrum of each substrate prior to the deposition of MoS_2.

Table 1: Binding energies of the main XPS peaks.

Substrate	S $2p_{3/2}$	S $2p_{1/2}$	S 2s	Mo $3d_{5/2}$	Mo $3d_{3/2}$	Mo $3p_{3/2}$	Mo $3p_{1/2}$	N 1s
SiO_2(nat)/Si	162.3	163.5	226.7	229.5	232.6	395.5	413.1	399.0
SiO_2(285 nm)/Si	162.3	163.5	226.7	229.5	232.6	395.5	413.0	399.2
PDMS	162.3	163.5	226.7	229.5	232.7	395.6	413.3	399.8
Silica	162.3	163.5	226.8	229.5	232.6	395.6	413.0	400.4

Raman and PL measurements can be exploited to gain insights into the presence of defects[55,56], strain[57,58] and doping[59,60] in monolayer flakes. Figure 5 shows representative Raman and PL spectra of the samples on each substrate. The in-plane E^1_{2g} and the out-of-plane A_{1g} Raman modes frequency are compatible with the typical values found in the literature. The frequency difference between the two modes was found at values ranging

View Article Online
DOI: 10.1039/D5NA00919G

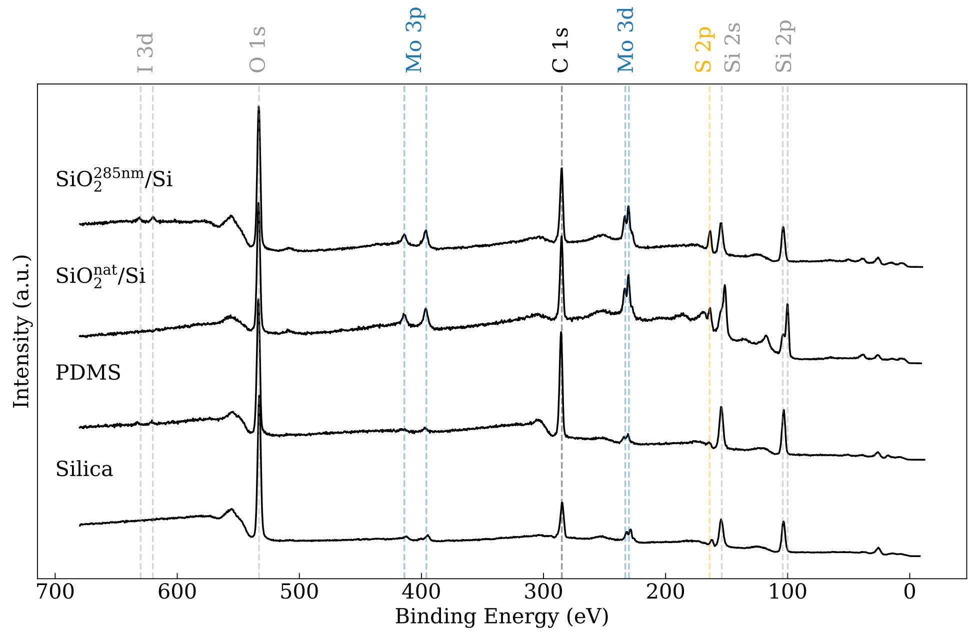

(a)

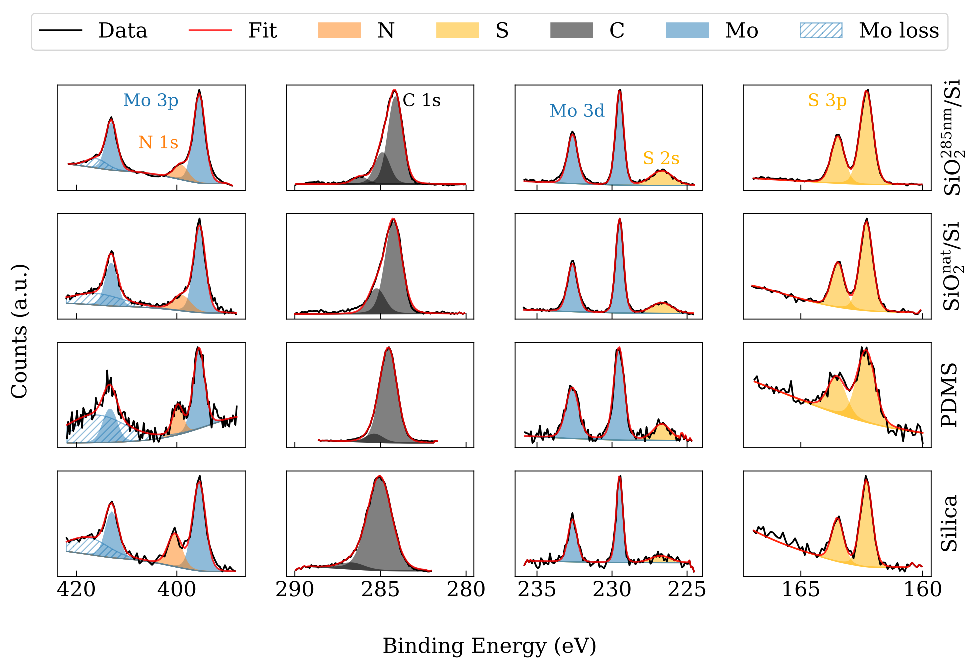

(b)

Figure 4: (a) XPS survey spectra of the samples on the different substrates. Vertical dashed lines have been added as a guide to the eye for tracing the major XPS peaks present in the spectra. (b) HR measurements performed on the the Mo 3d, Mo 3p, N 1s, C 1s and S 2p energy regions. Each row corresponds a different substrate labelled on the right side of the figure.

View Article Online
DOI: 10.1039/D5NA00919G

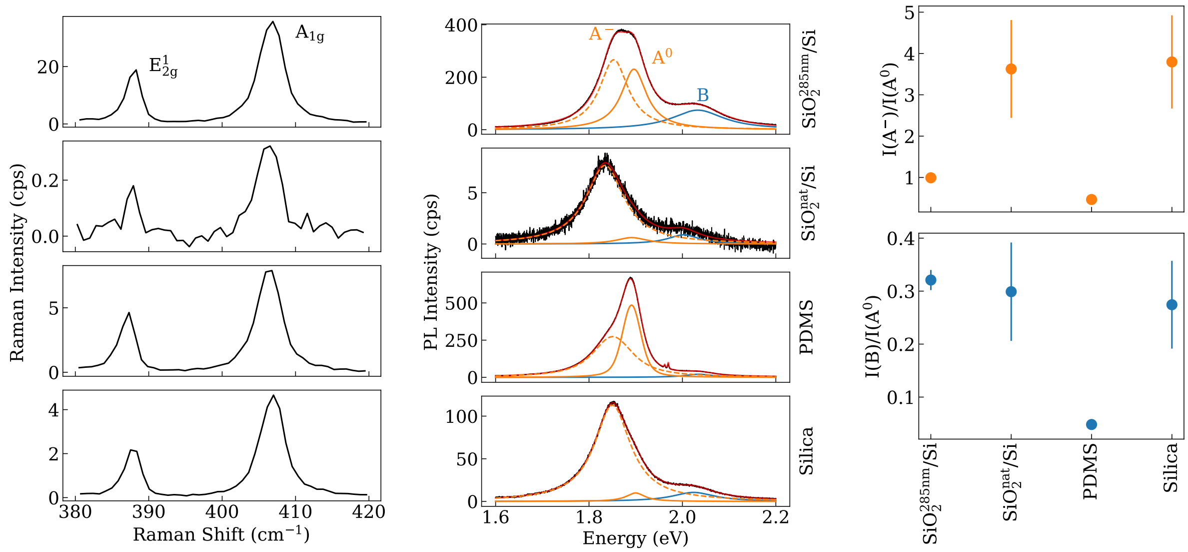

(a) (b) (c)

Figure 5: (a) Raman and (b) photoluminescence spectra. The black line show the background-subtracted experimental data. In the PL plots, orange solid and dashed lines and a blue solid line indicate the fitted A^0 exciton, A^- trion and B exciton peaks respectively. A solid red line shows the complete fitting function. (c) $I(B)/I(A^0)$ (bottom) and $I(A^-)/I(A^0)$ (top) intensity ratios extracted from the distributions in Figure S7.

from $\sim$ 18.6 cm^{-1} to $\sim$ 19.5 cm^{-1} for all the samples, fully compatible with monolayer MoS_2 samples. PL spectra, reported in Figure 5b, show clear differences depending on the target substrates, in particular with regard to the relative spectral weights of neutral exciton, trion and B-exciton contributions. When looking at the A exciton ($\sim$ 1.9 eV) and the A^- trion ($\sim$ 1.85 eV) we observe a strong variation of the peaks intensity ratio $I(A^-)/I(A^0)$ among samples. Figure 5c shows the mean value and deviation of the neutral-exciton/trion ratio for each substrate, with each measurement resulting from the average of over 500 points (the full distribution of the parameters is shown in Figure S7). We can easily notice that the PDMS sample features a substantially lower $I(A^-)/I(A^0)$ ratio when compared to the other samples, a difference compatible either with the presence of defects, or with low substrate-induced doping. In the case that defects gave the larger contribution, however, also the intensity ratio of the A and B excitons $I(B)/I(A^0)$ should increase[55], but the data show that the B exciton intensity on PDMS is very weak compared to that of the A

View Article Online
DOI: 10.1039/D5NA00919G

exciton, resulting in the low $I(B)/I(A^0)$ ratio observed in Figure 5c. As a consequence, the difference between the PL spectra of the PDMS sample and the other ones can be assigned to a lower substrate-induced doping of the MoS_2 in the PDMS case. On the contrary, the higher $I(A^-)/I(A^0)$ ratio observed in all the remaining samples, indicate higher electron doping levels, as indeed observed in MoS_2 samples deposited on silicon oxide surfaces[61–66]. A detailed characterization of the substrate induced doping effect was beyond the scope of this work.

Finally, we notice that both PL and Raman spectra on the native-oxide Si exhibit low signals compared to other samples, despite being acquired under analogous experimental conditions. Since both Raman and PL spectra do not significantly differ from those of MoS_2 on silica or thermal-oxide Si, we suggest that such a reduced signal might originate from dielectric screening and charge transfer effects between MoS_2 and the underlying Si. While, to our knowledge, there are no studies that directly involve PL and Raman measurements of MoS_2 on Si substrates, our hypothesis is supported by several studies of TMDCs on semiconducting and metallic surfaces[30,67–70] showing the quenching of the MoS_2 PL due to charge transfer and dielectric screening effects.

Deterministic transfer from PDMS stamps

The successful exfoliation of large-area flakes on PDMS opens up interesting perspectives, since PDMS is widely employed as a vector for the deterministic transfer of TMDC flakes onto a large variety of substrates[42,43]. It would, therefore, be extremely appealing to replicate such procedures with the very large flakes that we fabricate, thereby extending the range of possible target substrates to systems not currently compatible with the above-reported exfoliation technique, like noble-metal films. Furthermore, several applications of TMDCs, such as vdW heterostructures for electronics or optoelectronics require deterministic transfer approaches, that are intrinsically not guaranteed by the exfoliation process alone. In this

View Article Online
DOI: 10.1039/D5NA00919G

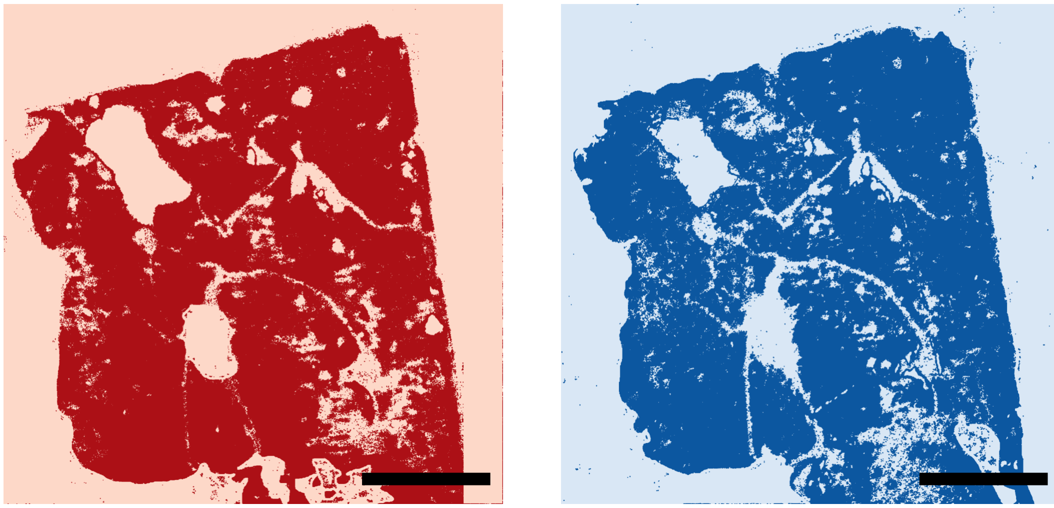

(a) Before transfer (b) After transfer

Figure 6: Binary maps extracted from the optical images in Figure S8 of the sample exfoliated on PDMS before (a) and after (b) its transfer on a SiO_2(nat)/Si substrate. The darker colours in both images correspond to areas identified as MoS_2. The scale bar is 250 µm.

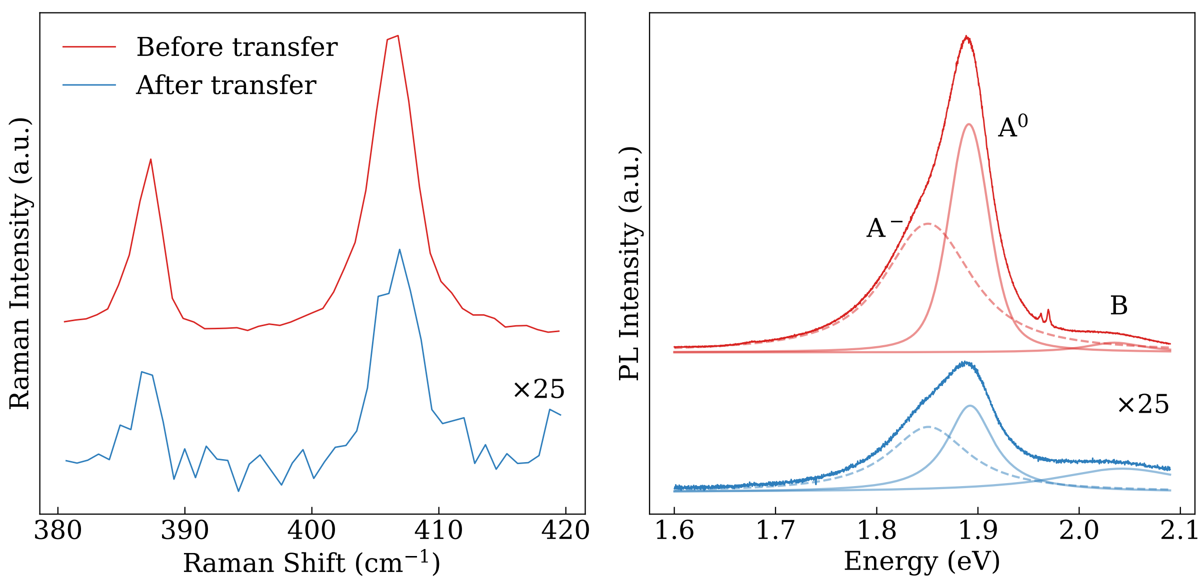

Figure 7: Characteristic Raman (left) and PL (right) spectra of the transferred sample before and after the transfer. The intensity of the spectra of the transferred sample was multiplied by a factor 25.

View Article Online
DOI: 10.1039/D5NA00919G

section we demonstrate the deterministic transfer of MoS_2 on a given substrate, adapting a common all dry-transfer method[42], performing a successful transfer on SiO_2(nat)/Si of our sample exfoliated on PDMS (Figure 2c).

In Figure 6 we show a binary intensity map of the sample before and after the transfer, constructed by identifying the MoS_2 regions in the corresponding optical images (Figure S8). We can observe that the original sample (Figure 6a) is almost entirely transferred on the target substrate (Figure 6b). Partial fragmentation is observed in localized region of the sample, however large uniform areas are still present after the sample is transferred.

The sample was then characterized by Raman and PL spectroscopy in order to asses its properties after the transfer. In Figure 7 we compare the spectra acquired before and after performing the transfer. We can observe that the spectroscopic features of the MoS_2 are hardly affected by the sample transfer. We observe, however, a significant reduction of both the Raman and PL intensities after transfer, comparable to what is observed with the sample directly produced on SiO_2(nat)/Si of Figure 2b. With a similar argument to that provided in the previous section, we can trace back this quenching effect to the interaction of the MoS_2 sample with the underlying silicon substrate, rather than being an intrinsic feature of the transferred MoS_2. Finally, we observe that the transferred sample features a lower $I(A^-)/I(A^0)$ ratio compared the one observed using the same substrate in Figure 5b. This can indicate that the interaction between the substrate and the MoS_2 is partially reduced due to contaminants associated with the PDMS transfer procedure[53,71].

Several other transfer attempts were performed on different substrates, to demonstrate the potential of combining our large-area exfoliation method with the PDMS dry-transfer technique. In SI we report two representative cases of flakes transferred on noteworthy substrates such as Si_3N_4 ultra-thin membrane used for TEM measurement (Figure S9) and optical microcavities nanofabricated on a silver film on CaF_2 (Figure S10).

View Article Online
DOI: 10.1039/D5NA00919G

Conclusions

In the present work we report a groundbreaking improvement of the previously reported gold-assisted mechanical exfoliation of bulk MoS_2. This method allowed to obtain millimeter-sized flakes on four substrates different from one another and representative of various fields of electronics and optoelectronics developments. In particular, the modification of one of the exfoliation steps, introducing a PDMS layer mechanically constraining the TRT during the release phase, allowed to increase the reliability of the exfoliation and enabled its generalization to different substrates. The key advantages of our method are its simplicity, scalability, reliability, cost-effectiveness and quickness. Uniquely, the exfoliation can be performed onto a wide range of target substrates without modifying the exfoliation procedure. Notably, the gold-assisted exfoliation of large MoS_2 samples on PDMS has been demonstrated. PDMS is a resourceful substrate material that enabled us to perform further deterministic transfers of the freshly exfoliated, millimeter-sized samples on desired substrates with micrometric control of the positioning of the 2D material.

Imaging ellipsometry has been employed to assess the local MoS_2 thickness over large-areas, thus enabling a fast and reliable determination of the monolayer nature of our exfoliated flakes. Moreover, our samples were characterized by Raman and photoluminescence spectroscopy in order to grade the quality and uniformity of the exfoliated samples. We observed substrate-dependent variations of the spectral features of the MoS_2 samples, which were identified as due to substrate-MoS_2 interactions. Overall, a high photoluminescence yield is observed, indicating high-quality monolayer samples. A Raman and photoluminescence quenching effect for the sample on SiO_2(nat)/Si was traced back to substrate/MoS_2 interactions, as well as intensity and PL peak shifts between different substrates.

The presented methodology represents a major breakthrough in the production of 2D material. We believe that its flexibility and scalability will drive major advancements in the fabrication of macroscopic 2D devices, ultimately enabling the complete exploitation of the exceptional properties of 2D materials.

View Article Online
DOI: 10.1039/D5NA00919G

Methods

Imaging Spectroscopic Ellipsometry (iSE) measurements were performed by means of a Park Systems Accurion EP4 imaging ellipsometer equipped with a laser-stabilized Xenon lamp and a monochromator. We acquired all our spectra in the 360 nm to 1000 nm range at an angle of incidence of 50° in rotating compensator mode. A 5× objective was used to focus the collected light to a CCD detector, simultaneously acquiring the whole probed area. Knife-edge illumination was used to block backside reflections and accurately measure the ellipsometric quantities on double-polished transparent substrates (PDMS and silica).

XPS spectra were acquired using a Physical Electronics PHI 5600 photoelectron spectrometer, equipped with a monochromatized Al K_α source and with an electron flood gun to reduce surface charging. Once acquired, XPS spectra were corrected for charging effects by using the C 1s peak of carbon at 284.8 eV as a reference. XPS data analysis was performed using the CasaXPS software. The spectra were fitted using the symmetric Voigt-like LA(1.53, 243) line shape in CasaXPS. The S 2p, Mo 3p, and Mo 3d doublets were fitted while keeping the $p_{3/2}$:$p_{1/2}$ and $d_{5/2}$:$d_{3/2}$ area ratios fixed at 2:1 and 3:2, respectively. The S 2p spin-orbit peaks were also constrained to have the same full-width at half-maximum (FWHM). The Mo 3p and Mo 3d spin-orbit peaks were allowed to have different FHWM to better reproduce the experimental data. The need of non-identical FWHM to fit the Mo doublets is due to the Coster-Kronig broadening, which has been observed on similar compounds[72–74]. The C 1s peak has been fitted with two components with the same FWHM, except for the sample on SiO_2(285 nm)/Si, where the spectral lineshape clearly suggests a third component at higher binding energies, which can be attributed to additional contamination.

Micro Raman and photoluminescence spectroscopy was performed using a Jasco NRS-4100 Raman spectrometer. The probing laser was a 532 nm laser filtered to have ∼ 100 µW of power on the sample through a 100×, 0.9 NA objective. A 2400 grooves/mm grating was used to disperse scattered light for the Raman measurements; a 900 grooves/mm grating was used for photoluminescence measurements.

View Article Online
DOI: 10.1039/D5NA00919G

Acknowledgements

We thank doctor N. Petrini and professor I. Kriegel for the critical reading of the manuscript.

This work was carried out within the framework of the project "RAISE - Robotics and AI for Socio-economic Empowerment" and has been supported by European Union - NextGenerationEU. Funded by the European Union - NextGenerationEU. However, the views and opinions expressed are hose of the authors alone and do not necessarily reflect those of the European Union or the European Commission. Neither the European Union nor the European Commission can be held responsible for them.

Data availability

The datasets analysed during the current study are available at https://doi.org/10.5281/zenodo.17602072.

References

(1) Novoselov, K. S.; Geim, A. K.; Morozov, S. V.; Jiang, D.; Zhang, Y.; Dubonos, S. V.; Grigorieva, I. V.; Firsov, A. A. Electric Field Effect in Atomically Thin Carbon Films. *Science* **2004**, *306*, 666–669.

(2) Novoselov, K. S.; Mishchenko, A.; Carvalho, A.; Neto, A. H. C. 2D materials and van der Waals heterostructures. *Science* **2016**, *353*, aac9439.

(3) Manzeli, S.; Ovchinnikov, D.; Pasquier, D.; Yazyev, O. V.; Kis, A. 2D transition metal dichalcogenides. *Nat. Rev. Mater.* **2017**, *2*, 1–15.

(4) Splendiani, A.; Sun, L.; Zhang, Y.; Li, T.; Kim, J.; Chim, C.-Y.; Galli, G.; Wang, F. Emerging Photoluminescence in Monolayer MoS_2. *Nano Lett.* **2010**, *10*, 1271–1275.

View Article Online
DOI: 10.1039/D5NA00919G

(5) Chernikov, A.; Berkelbach, T. C.; Hill, H. M.; Rigosi, A.; Li, Y.; Aslan, B.; Reichman, D. R.; Hybertsen, M. S.; Heinz, T. F. Exciton Binding Energy and Nonhydrogenic Rydberg Series in Monolayer WS_2. *Phys. Rev. Lett.* **2014**, *113*, 076802.

(6) Mak, K. F.; He, K.; Shan, J.; Heinz, T. F. Control of valley polarization in monolayer MoS_2 by optical helicity. *Nat. Nanotechnol.* **2012**, *7*, 494–498.

(7) Jariwala, D.; Sangwan, V. K.; Lauhon, L. J.; Marks, T. J.; Hersam, M. C. Emerging Device Applications for Semiconducting Two-Dimensional Transition Metal Dichalcogenides. *ACS Nano* **2014**, *8*, 1102–1120.

(8) Wang, G.; Chernikov, A.; Glazov, M. M.; Heinz, T. F.; Marie, X.; Amand, T.; Urbaszek, B. Colloquium: Excitons in atomically thin transition metal dichalcogenides. *Rev. Mod. Phys.* **2018**, *90*, 021001.

(9) Raza, A.; Hassan, J. Z.; Ikram, M.; Ali, S.; Farooq, U.; Khan, Q.; Maqbool, M. Advances in Liquid-Phase and Intercalation Exfoliations of Transition Metal Dichalcogenides to Produce 2D Framework. *Adv. Mater. Interfaces* **2021**, *8*, 2002205.

(10) Lee, Y.-H.; Zhang, X.-Q.; Zhang, W.; Chang, M.-T.; Lin, C.-T.; Chang, K.-D.; Yu, Y.-C.; Wang, J. T.-W.; Chang, C.-S.; Li, L.-J.; Lin, T.-W. Synthesis of Large-Area MoS2 Atomic Layers with Chemical Vapor Deposition. *Adv. Mater.* **2012**, *24*, 2320–2325.

(11) Wang, Q. et al. Wafer-Scale Highly Oriented Monolayer MoS2 with Large Domain Sizes. *Nano Lett.* **2020**, *20*, 7193–7199.

(12) Chubarov, M.; Choudhury, T. H.; Hickey, D. R.; Bachu, S.; Zhang, T.; Sebastian, A.; Bansal, A.; Zhu, H.; Trainor, N.; Das, S.; Terrones, M.; Alem, N.; Redwing, J. M. Wafer-Scale Epitaxial Growth of Unidirectional WS2 Monolayers on Sapphire. *ACS Nano* **2021**, *15*, 2532–2541.

View Article Online
DOI: 10.1039/D5NA00919G

(13) Yang, P. et al. Epitaxial Growth of Centimeter-Scale Single-Crystal MoS2 Monolayer on Au(111). *ACS Nano* **2020**, *14*, 5036–5045.

(14) Jiang, H.; Zhang, X.; Chen, K.; He, X.; Liu, Y.; Yu, H.; Gao, L.; Hong, M.; Wang, Y.; Zhang, Z.; Zhang, Y. Two-dimensional Czochralski growth of single-crystal MoS2. *Nat. Mater.* **2025**, *24*, 188–196.

(15) Velický, M. et al. Mechanism of Gold-Assisted Exfoliation of Centimeter-Sized Transition-Metal Dichalcogenide Monolayers. *ACS Nano* **2018**, *12*, 10463–10472.

(16) Magda, G. Z.; Pető, J.; Dobrik, G.; Hwang, C.; Biró, L. P.; Tapasztó, L. Exfoliation of large-area transition metal chalcogenide single layers. *Sci. Rep.* **2015**, *5*, 14714.

(17) Desai, S. B.; Madhvapathy, S. R.; Amani, M.; Kiriya, D.; Hettick, M.; Tosun, M.; Zhou, Y.; Dubey, M.; Ager, J. W.; Chrzan, D.; Javey, A. Gold-mediated exfoliation of ultralarge optoelectronically-perfect monolayers. *Adv. Mater.* **2016**, *28*, 4053–4058.

(18) Liu, F. Mechanical exfoliation of large area 2D materials from vdW crystals. *Prog. Surf. Sci.* **2021**, *96*, 100626.

(19) Heyl, M.; List-Kratochvil, E. J. Only gold can pull this off: mechanical exfoliations of transition metal dichalcogenides beyond scotch tape. *Appl. Phys. A* **2023**, *129*, 16.

(20) Panasci, S. E.; Schilirò, E.; Roccaforte, F.; Giannazzo, F. Gold-Assisted Exfoliation of Large-Area Monolayer Transition Metal Dichalcogenides: From Interface Properties to Device Applications. *Adv. Funct. Mater.* **2025**, *35*, 2414532.

(21) Sahu, S.; Haider, G.; Rodriguez, A.; Plšek, J.; Mergl, M.; Kalbáč, M.; Frank, O.; Velický, M. Large-Area Mechanically-Exfoliated Two-Dimensional Materials on Arbitrary Substrates. *Adv. Mater. Technol.* **2023**, *8*, 2201993.

View Article Online
DOI: 10.1039/D5NA00919G

(22) Olsen, N. et al. Macroscopic Transition Metal Dichalcogenide Monolayers from Gold-Tape Exfoliation Retain Intrinsic Properties. *Nano Lett.* **2025**, *25*, 15198–15205, PMID: 41071051.

(23) Heyl, M.; Burmeister, D.; Schultz, T.; Pallasch, S.; Ligorio, G.; Koch, N.; List-Kratochvil, E. J. W. Thermally Activated Gold-Mediated Transition Metal Dichalcogenide Exfoliation and a Unique Gold-Mediated Transfer. *Phys. Status Solidi RRL* **2020**, *14*, 2000408.

(24) Pirker, L.; Honolka, J.; Velický, M.; Frank, O. When 2D materials meet metals. *2D Mater.* **2024**, *11*, 022003.

(25) Huang, Y. et al. Universal mechanical exfoliation of large-area 2D crystals. *Nat. Commun.* **2020**, *11*, 2453.

(26) Huang, X.; Zhang, L.; Liu, L.; Qin, Y.; Fu, Q.; Wu, Q.; Yang, R.; Lv, J.-P.; Ni, Z.; Liu, L.; Ji, W.; Wang, Y.; Zhou, X.; Huang, Y. Raman spectra evidence for the covalent-like quasi-bonding between exfoliated MoS_2 and Au films. *Sci. China Inf. Sci.* **2021**, *64*, 140406.

(27) Hanušová, M. et al. Hybridization Directionality Governs the Interaction Strength between MoS2 and Metals. *Nano Lett.* **2025**, *25*, 12995–13002.

(28) Farmanbar, M.; Brocks, G. First-principles study of van der Waals interactions and lattice mismatch at MoS_2/metal interfaces. *Phys. Rev. B* **2016**, *93*, 085304.

(29) Velický, M.; Rodriguez, A.; Bouša, M.; Krayev, A. V.; Vondráček, M.; Honolka, J.; Ahmadi, M.; Donnelly, G. E.; Huang, F.; Abruña, H. D.; Novoselov, K. S.; Frank, O. Strain and Charge Doping Fingerprints of the Strong Interaction between Monolayer MoS2 and Gold. *J. Phys. Chem. Lett.* **2020**, *11*, 6112–6118.

View Article Online
DOI: 10.1039/D5NA00919G

(30) Pollmann, E.; Sleziona, S.; Foller, T.; Hagemann, U.; Gorynski, C.; Petri, O.; Madauß, L.; Breuer, L.; Schleberger, M. Large-Area, Two-Dimensional MoS2 Exfoliated on Gold: Direct Experimental Access to the Metal–Semiconductor Interface. *ACS Omega* **2021**, *6*, 15929–15939.

(31) Panasci, S. E.; Schilirò, E.; Greco, G.; Cannas, M.; Gelardi, F. M.; Agnello, S.; Roccaforte, F.; Giannazzo, F. Strain, Doping, and Electronic Transport of Large Area Monolayer MoS_2 Exfoliated on Gold and Transferred to an Insulating Substrate. *ACS Appl. Mater. Interfaces* **2021**, *13*, 31248–31259.

(32) Rodriguez, A.; Velický, M. c. v.; Řáhová, J.; Zólyomi, V.; Koltai, J.; Kalbáč, M.; Frank, O. Activation of Raman modes in monolayer transition metal dichalcogenides through strong interaction with gold. *Phys. Rev. B* **2022**, *105*, 195413.

(33) Sun, H.; Sirott, E. W.; Mastandrea, J.; Gramling, H. M.; Zhou, Y.; Poschmann, M.; Taylor, H. K.; Ager, J. W.; Chrzan, D. C. Theory of thin-film-mediated exfoliation of van der Waals bonded layered materials. *Phys. Rev. Mater.* **2018**, *2*, 094004.

(34) Ziewer, J.; Ghosh, A.; Hanušová, M.; Pirker, L.; Frank, O.; Velický, M.; Grüning, M.; Huang, F. Strain-Induced Decoupling Drives Gold-Assisted Exfoliation of Large-Area Monolayer 2D Crystals. *Adv. Mater.* **2025**, *37*, 2419184.

(35) Corletto, A.; Fronzi, M.; Joannidis, A. K.; Sherrell, P. C.; Ford, M. J.; Winkler, D. A.; Shapter, J. G.; Bullock, J.; Ellis, A. V. A Predictive Model for Monolayer-Selective Metal-Mediated MoS_2 Exfoliation Incorporating Electrostatics. *Adv. Mater. Interfaces* **2024**, *11*, 2300686.

(36) Johnston, A. C.; Khondaker, S. I. Can Metals Other than Au be Used for Large Area Exfoliation of MoS_2 Monolayers? *Adv. Mater. Interfaces* **2022**, *9*, 2200106.

(37) Velický, M.; Donnelly, G. E.; Hendren, W. R.; DeBenedetti, W. J. I.; Hines, M. A.;

View Article Online
DOI: 10.1039/D5NA00919G

Novoselov, K. S.; Abruña, H. D.; Huang, F.; Frank, O. The Intricate Love Affairs between MoS_2 and Metallic Substrates. *Adv. Mater. Interfaces* **2020**, *7*, 2001324.

(38) Ding, S. et al. Ag-Assisted Dry Exfoliation of Large-Scale and Continuous 2D Monolayers. *ACS Nano* **2024**, *18*, 1195–1203.

(39) Liu, F.; Wu, W.; Bai, Y.; Chae, S. H.; Li, Q.; Wang, J.; Hone, J.; Zhu, X.-Y. Disassembling 2D van der Waals crystals into macroscopic monolayers and reassembling into artificial lattices. *Science* **2020**, *367*, 903–906.

(40) Petrini, N.; Peci, E.; Curreli, N.; Spotorno, E.; Kazemi Tofighi, N.; Magnozzi, M.; Scotognella, F.; Bisio, F.; Kriegel, I. Optimizing Gold-Assisted Exfoliation of Layered Transition Metal Dichalcogenides with (3-Aminopropyl)triethoxysilane (APTES): A Promising Approach for Large-Area Monolayers. *Adv. Opt. Mater.* **2024**, 2303228.

(41) Ramò, L.; Peci, E.; Magnozzi, M.; Spotorno, E.; Venturino, V.; Sygletou, M.; Giordano, M. C.; Zambito, G.; Telesio, F.; Milosz, Z.; Canepa, M.; Bisio, F. Noninvasive Deterministic Nanostructures Lithography on 2D Transition Metal Dichalcogenides. *Adv. Eng. Mater.* **2025**, *27*, 2401157.

(42) Castellanos-Gomez, A.; Buscema, M.; Molenaar, R.; Singh, V.; Janssen, L.; van der Zant, H. S. J.; Steele, G. A. Deterministic transfer of two-dimensional materials by all-dry viscoelastic stamping. *2D Mater.* **2014**, *1*, 011002.

(43) Watson, A. J.; Lu, W.; Guimarães, M. H. D.; Stöhr, M. Transfer of large-scale two-dimensional semiconductors: challenges and developments. *2D Mater.* **2021**, *8*, 032001.

(44) Velický, M. et al. Mechanism of Gold-Assisted Exfoliation of Centimeter-Sized Transition-Metal Dichalcogenide Monolayers. *ACS Nano* **2018**, *12*, 10463–10472.

(45) Fu, Q. et al. One-Step Exfoliation Method for Plasmonic Activation of Large-Area 2D Crystals. *Adv. Sci.* **2022**, *9*, 2204247.

View Article Online
DOI: 10.1039/D5NA00919G

(46) Haider, G.; Gastaldo, M.; Karim, B.; Plšek, J.; Varade, V.; Volochanskyi, O.; Vejpravová, J.; Kalbáč, M. Highly Efficient Bulk-Crystal-Sized Exfoliation of 2D Materials under Ultrahigh Vacuum. *ACS Appl. Electron. Mater.* **2024**, *6*, 2301–2308.

(47) Peci, E.; Magnozzi, M.; Ramò, L.; Ferrera, M.; Convertino, D.; Pace, S.; Orlandini, G.; Sharma, A.; Milekhin, I.; Salvan, G.; Coletti, C.; Zahn, D. R. T.; Bisio, F.; Canepa, M. Dielectric Function of 2D Tungsten Disulfide in Homo- and Heterobilayer Stacking. *Adv. Mater. Interfaces* **2023**, *10*, 2201586.

(48) Magnozzi, M.; Pflug, T.; Ferrera, M.; Pace, S.; Ramó, L.; Olbrich, M.; Canepa, P.; Ağircan, H.; Horn, A.; Forti, S.; Cavalleri, O.; Coletti, C.; Bisio, F.; Canepa, M. Local Optical Properties in CVD-Grown Monolayer WS2 Flakes. *J. Phys. Chem. C* **2021**, *125*, 16059–16065.

(49) Magnozzi, M.; Ferrera, M.; Piccinini, G.; Pace, S.; Forti, S.; Fabbri, F.; Coletti, C.; Bisio, F.; Canepa, M. Optical dielectric function of two-dimensional WS2 on epitaxial graphene. *2D Mater.* **2020**, *7*, 025024.

(50) Funke, S.; Miller, B.; Parzinger, E.; Thiesen, P.; Holleitner, A. W.; Wurstbauer, U. Imaging spectroscopic ellipsometry of MoS_2. *J. Phys. Condens. Matter* **2016**, *28*, 385301.

(51) Peci, E.; Petrini, N.; Curreli, N.; Spotorno, E.; Tofighi, N. K.; Magnozzi, M.; Scotognella, F.; Kriegel, I.; Bisio, F. Fast thickness mapping of large-area exfoliated two-dimensional transition metal dichalcogenides by imaging spectroscopic ellipsometry. *EPJ Web Conf.* **2024**, *309*, 06006.

(52) Shearer, C. J.; Slattery, A. D.; Stapleton, A. J.; Shapter, J. G.; Gibson, C. T. Accurate thickness measurement of graphene. *Nanotechnology* **2016**, *27*, 125704.

(53) Pan, Y.; Zahn, D. R. T. Raman Fingerprint of Interlayer Coupling in 2D TMDCs. *Nanomaterials* **2022**, *12*.

View Article Online
DOI: 10.1039/D5NA00919G

(54) Greczynski, G.; Hultman, L. Binding energy referencing in X-ray photoelectron spectroscopy. *Nat. Rev. Mat.* **2025**, *10*, 62–78.

(55) McCreary, K. M.; Hanbicki, A. T.; Sivaram, S. V.; Jonker, B. T. A- and B-exciton photoluminescence intensity ratio as a measure of sample quality for transition metal dichalcogenide monolayers. *APL Mater.* **2018**, *6*, 111106.

(56) Sousa, F. B.; Nadas, R.; Martins, R.; Barboza, A. P. M.; Soares, J. S.; Neves, B. R. A.; Silvestre, I.; Jorio, A.; Malard, L. M. Disentangling doping and strain effects at defects of grown MoS2 monolayers with nano-optical spectroscopy. *Nanoscale* **2024**, *16*, 12923–12933.

(57) Liu, Z. et al. Strain and structure heterogeneity in MoS2 atomic layers grown by chemical vapour deposition. *Nat. Commun.* **2014**, *5*, 5246.

(58) Castellanos-Gomez, A.; Roldán, R.; Cappelluti, E.; Buscema, M.; Guinea, F.; van der Zant, H. S. J.; Steele, G. A. Local Strain Engineering in Atomically Thin MoS2. *Nano Lett.* **2013**, *13*, 5361–5366.

(59) Vaquero, D.; Clericò, V.; Salvador-Sánchez, J.; Martín-Ramos, A.; Díaz, E.; Domínguez-Adame, F.; Meziani, Y. M.; Diez, E.; Quereda, J. Excitons, trions and Rydberg states in monolayer MoS2 revealed by low-temperature photocurrent spectroscopy. *Commun. Phys.* **2020**, *3*, 194.

(60) Mouri, S.; Miyauchi, Y.; Matsuda, K. Tunable Photoluminescence of Monolayer MoS2 via Chemical Doping. *Nano Lett.* **2013**, *13*, 5944–5948.

(61) Scheuschner, N.; Ochedowski, O.; Kaulitz, A.-M.; Gillen, R.; Schleberger, M.; Maultzsch, J. Photoluminescence of freestanding single- and few-layer MoS_2. *Phys. Rev. B* **2014**, *89*, 125406.

View Article Online
DOI: 10.1039/D5NA00919G

(62) Buscema, M.; Steele, G. A.; van der Zant, H. S. J.; Castellanos-Gomez, A. The effect of the substrate on the Raman and photoluminescence emission of single-layer MoS2. *Nano Res.* **2014**, *7*, 561–571.

(63) Chae, W. H.; Cain, J. D.; Hanson, E. D.; Murthy, A. A.; Dravid, V. P. Substrate-induced strain and charge doping in CVD-grown monolayer MoS2. *Appl. Phys. Lett.* **2017**, *111*, 143106.

(64) Fan, X.; Nouchi, R.; Tanigaki, K. Effect of Charge Puddles and Ripples on the Chemical Reactivity of Single Layer Graphene Supported by SiO2/Si Substrate. *J. Phys. Chem. C* **2011**, *115*, 12960–12964.

(65) Ji, E.; Kim, M. J.; Lee, J.-Y.; Sung, D.; Kim, N.; Park, J.-W.; Hong, S.; Lee, G.-H. Substrate effect on doping and degradation of graphene. *Carbon* **2021**, *184*, 651–658.

(66) Sun, Y.; Wang, R.; Liu, K. Substrate induced changes in atomically thin 2-dimensional semiconductors: Fundamentals, engineering, and applications. *Appl. Phys. Rev.* **2017**, *4*, 011301.

(67) Rojas-Lopez, R. R.; Brant, J. C.; Ramos, M. S. O.; Castro, T. H. L. G.; Guimarães, M. H. D.; Neves, B. R. A.; Guimarães, P. S. S. Photoluminescence and charge transfer in the prototypical 2D/3D semiconductor heterostructure MoS2/GaAs. *Appl. Phys. Lett.* **2021**, *119*, 233101.

(68) Panasci, S. E.; Schilirò, E.; Migliore, F.; Cannas, M.; Gelardi, F. M.; Roccaforte, F.; Giannazzo, F.; Agnello, S. Substrate impact on the thickness dependence of vibrational and optical properties of large area MoS2 produced by gold-assisted exfoliation. *Appl. Phys. Lett.* **2021**, *119*, 093103.

(69) Bhanu, U.; Islam, M. R.; Tetard, L.; Khondaker, S. I. Photoluminescence quenching in gold - MoS2 hybrid nanoflakes. *Sci. Rep.* **2014**, *4*, 5575.

View Article Online
DOI: 10.1039/D5NA00919G

(70) Hossain, M. T.; Mawlong, L. P. L.; Jena, T.; Bora, A.; Nath, U.; Sarma, M.; Giri, P. K. Interlayer Charge-Transfer-Induced Photoluminescence Quenching and Enhanced Photoconduction in Two-Dimensional Bi2O2Se/MoS2 Type-II Heterojunction. *ACS Appl. Nano Mater.* **2023**, *6*, 11023–11036.

(71) Haigh, S. J.; Gholinia, A.; Jalil, R.; Romani, S.; Britnell, L.; Elias, D. C.; Novoselov, K. S.; Ponomarenko, L. A.; Geim, A. K.; Gorbachev, R. Cross-sectional imaging of individual layers and buried interfaces of graphene-based heterostructures and superlattices. *Nat. Mater.* **2012**, *11*, 764–767.

(72) Nolot, E.; Cadot, S.; Martin, F.; Hönicke, P.; Zech, C.; Beckhoff, B. In-line characterization of ultrathin transition metal dichalcogenides using X-ray fluorescence and X-ray photoelectron spectroscopy. *Spectrochim. Acta B* **2020**, *166*, 105788.

(73) Jones, L. A. H.; Xing, Z.; Swallow, J. E. N.; Shiel, H.; Featherstone, T. J.; Smiles, M. J.; Fleck, N.; Thakur, P. K.; Lee, T.-L.; Hardwick, L. J.; Scanlon, D. O.; Regoutz, A.; Veal, T. D.; Dhanak, V. R. Band Alignments, Electronic Structure, and Core-Level Spectra of Bulk Molybdenum Dichalcogenides (MoS_2, $MoSe_2$, and $MoTe_2$). *J. Phys. Chem. C* **2022**, *126*, 21022–21033.

(74) Mårtensson, N.; Nyholm, R. Electron spectroscopic determinations of M and N core-hole lifetimes for the elements Nb–Te (Z=41–52). *Phys. Rev. B* **1981**, *24*, 7121.

View Article Online
DOI: 10.1039/D5NA00919G

The datasets analysed during the current study are available at https://doi.org/10.5281/zenodo.17602072.